



ELSEVIER

Available online at [www.sciencedirect.com](http://www.sciencedirect.com)

SCIENCE @ DIRECT®

Materials Letters 57 (2003) 1604–1611

**MATERIALS  
LETTERS**

[www.elsevier.com/locate/matlet](http://www.elsevier.com/locate/matlet)

# Synthesis of nanocrystalline SnO<sub>2</sub> powder by amorphous citrate route

Mahesh Bhagwat, Pallavi Shah, Veda Ramaswamy\*

*Inorganic Chemistry and Catalysis Division, National Chemical Laboratory, Pune 411008, Maharashtra, India*

Received 18 January 2002; received in revised form 20 June 2002; accepted 12 July 2002

## Abstract

Nanocrystalline SnO<sub>2</sub> has been synthesized by liquid mix technique using citric acid as the complexing agent. The tin oxide powder obtained at different calcination temperatures (773–1223 K) is characterized using powder X-ray diffraction (XRD), SEM, TEM, TG-DTG and UV spectroscopic techniques. The material obtained is nanocrystalline, having particle size in the range of 10–14 nm. The technique is cost-effective and yields the desired product at temperatures as low as 773 K.

© 2002 Elsevier Science B.V. All rights reserved.

*Keywords:* Tin oxide; Citric acid; Nanocrystalline; Citrate glass; Powder XRD; TEM

## 1. Introduction

Tin (IV) oxide has been a widely studied material over decades because of its wide range of applications as gas sensors, heat mirrors, transparent electrodes for solar cells, opto-electronic devices and in catalysis. SnO<sub>2</sub> semiconductors in the form of thick or thin films and powders have been studied as a promising gas sensor for a variety of noxious and explosive gases like CO, hydrocarbons, ethanol, ammonia, hydrogen, nitrogen oxides and hydrogen sulfide [1–6]. These gases remove oxide ions from the semiconductor, thus causing the resistance of the later to decrease considerably. The gas-induced resis-

tivity changes of SnO<sub>2</sub> strongly depend on particle size, size distribution and specific surface area of the powder, which in turn are governed by the technique used for the oxide preparation [5,7–9]. Properly prepared, nanometer sized particles might be used to form the high surface area analogues of known sensors to provide improved efficiency of sensor function. Due to its surface modification, application of nanostructured SnO<sub>2</sub> as an active material in gas sensing is known.

Among the various methods of preparing nanostructured SnO<sub>2</sub>, co-precipitation, sol–gel, spray-pyrolysis, hydrothermal routes, freeze-drying, etc., are popular. Recently, gel combustion routes using a variety of organic fuels like urea, hydrazine, citric acid and others have been reported to be promising methods to prepare a variety of oxides including nanocrystalline SnO<sub>2</sub> [9–16]. Though the combustion methods are fairly simple, higher calcination

\* Corresponding author. Fax: +91-20-589-3761.

E-mail address: [veda@cata.ncl.res.in](mailto:veda@cata.ncl.res.in) (V. Ramaswamy).

temperatures have been reported and the method requires an oxidizing agent and necessarily a fuel in the reaction mixture [17]. In the present work, we report the synthesis of nanostructured SnO<sub>2</sub> by liquid mix technique [18]. The technique is employed to synthesize nanocrystalline SnO<sub>2</sub> at relatively lower temperatures. The method is fast, relatively cost-effective and yields nanopowders with a fairly narrow particle size distribution.

The technique involves mixing of solutions of a metal precursor and an organic polyfunctional acid possessing at least one hydroxyl and one carboxylic acid group such as citric, malic, tartaric, glycolic or lactic which results in complexation of the metal by the polycarboxylic acid. Probable complex of a divalent metal cation and the citric acid is shown in Fig. 1 [19]. Slow heating of this mixture results in evaporation of the solvent to form a solution with increasing viscosity. After complete removal of the solvent, the dried product is in a rigid polymeric glassy state that is homogeneous and mixed at atomic level. This homogeneous glass is then calcined at relatively lower temperature to obtain sub-micron level particles. Combustion of the metal–acid complex is highly exothermic and provides large amount of heat for quick conversion into oxides. Since the complexation agent is behaving as a flux, addition of an extra material as a fuel is not required. This technique has been widely used a couple of decades ago for synthesis of simple as well as mixed

oxides [20–23]. However, no recent reports using this method for metal oxides synthesis could be found. We have prepared nanostructured SnO<sub>2</sub> particles by the liquid mix technique using citric acid as the complexing agent at relatively lower temperature (773 K). The nanocrystalline product obtained is carbon free at this temperature, whereas higher temperatures were required to remove carbon in earlier reports in which a similar synthesis method was used [19].

## 2. Experimental

The amorphous metal citrate glass was obtained by mixing saturated aqueous solutions of SnCl<sub>2</sub>·2H<sub>2</sub>O (99% pure, PCL, India) and citric acid (99.97% pure A.R. grade, S.D. Fine-Chem., India). As a part of the experimentation, three different mole ratios of the precursors were taken viz., 3:2, 3:5, and 3:8 with respect to Sn metal. The resultant mixtures were heated slowly on a hot plate at 80 °C to evaporate the solvent. On complete removal of water, the highly viscous mass turned into a transparent glass. It was observed that the mixture taken in a ratio of 3:2 did not form a good amorphous glass. Mixtures with the remaining two ratios, in which excess citric acid was taken, were used for the metal oxide synthesis which was divided into five equal parts. The five equal parts of the amorphous glass were taken in different alumina crucibles and calcined in a muffle furnace in air at a heating rate of 10 °C min<sup>-1</sup> at temperatures 773, 873, 973, 1073 and 1173 K, respectively, for 15 min, which resulted in the formation of loose off-white, well crystalline nanoparticles of SnO<sub>2</sub>.

The citrate glass and the samples calcined at various temperatures were characterized by powder X-ray diffraction (XRD) technique on a Rigaku D-Max III VC Powder XRD diffractometer using Ni filter, Cu K $\alpha$  radiation ( $\lambda=1.54056$  Å) and NaI scintillation counter detector. Silicon was used as an internal standard to correct the interplanar distance  $d$ . The samples were scanned in the range 20–100°  $2\theta$  for a period of 5 s in the step scan mode. The crystallite size measurements were carried out using the Scherrer equation,  $D=k\lambda/\beta\cos\theta$ , where  $D$  is the crystallite size,  $k$  is the Scherrer constant ( $=0.9$  assuming that the particles are spherical),  $\lambda$  is the

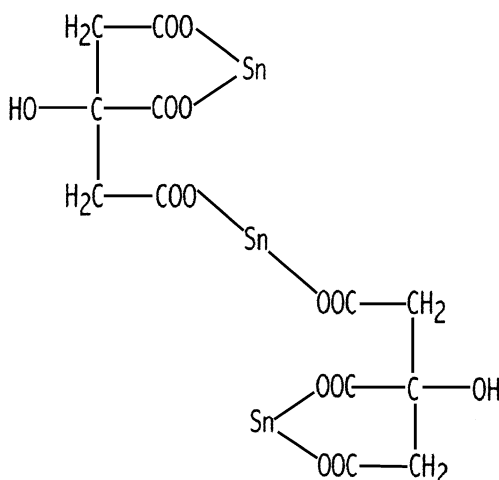


Fig. 1. Probable structure of the metal citrate structure.

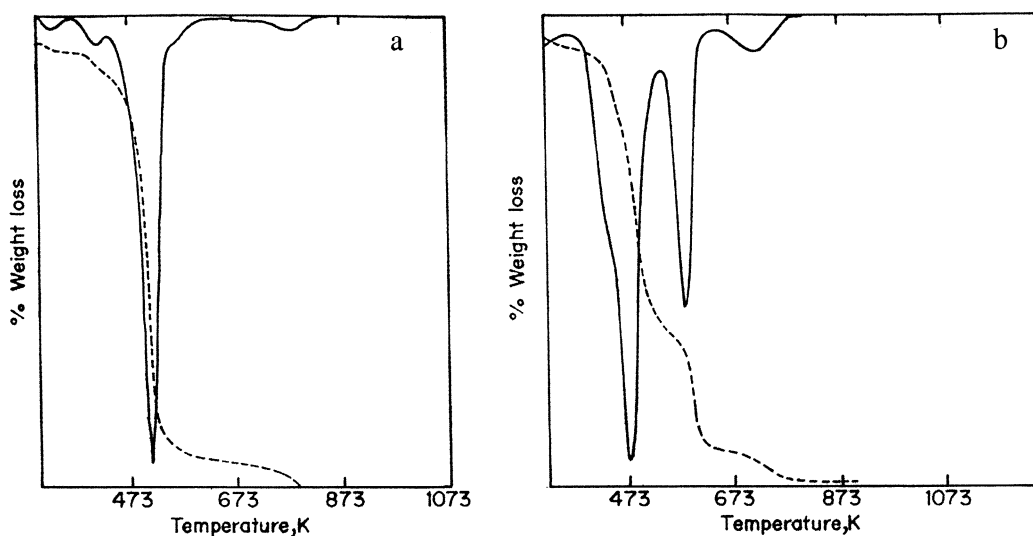


Fig. 2. (a) Thermogram of the citric acid used as the precursor. (b) Thermogram of the metal citrate glass.

wavelength of the X-ray radiation (Cu  $K\alpha$  radiation ( $\lambda = 1.54050 \text{ \AA}$ ),  $\beta$  is the line width (obtained after correction for the instrumental broadening is applied) and  $\theta$  is the diffraction peak angle. The lattice parameters were calculated using the corrected  $d$  values and the least square fitting. Specific surface area of the samples was calculated from the formula  $S = 6 \times 10^3 / d\rho$ , where  $S$  is the specific surface area ( $\text{m}^2/\text{g}$ ),  $d$  is the average crystallite size ( $\text{\AA}$ ) and  $\rho$  is the density of  $\text{SnO}_2$  ( $\text{cm}^3/\text{g}$ ). The samples were analyzed for the presence of carbon by microanalysis technique on a CARLO ELBA EA-1108 analyzer. SEM micrographs of the samples were recorded on a JOEL-JSM-5200 Scanning Electron Microscope to observe the morphology of the oxide particles. TEM measurements were carried out on a JEOL Model 1200EX instrument operated at an accelerating voltage of 100 kV. The thermogravimetric analysis of the citrate glass

and the precursor citric acid was carried out to monitor the nature of decomposition of both. Thermal analysis was done on a Setaram thermal analyzer (SETARAM) at a heating rate of  $10^\circ \text{ min}^{-1}$  in air atmosphere. Diffused reflectance ultraviolet visible spectra of the samples were recorded on a Shimadzu UV-Visible Spectrophotometer, UV-2550 PC using barium sulfate as the standard.

### 3. Results and discussions

Spherical particles of nanocrystalline  $\text{SnO}_2$  were obtained by the amorphous citrate route (liquid mix technique). During the calcination process, a black fluffy mass (foam-like) is formed which occupies large volumes of the furnace. As the temperature increases, the black mass turns to white in color with

Table 1

Weight loss at various steps as obtained from the thermal analysis data

Step no.	Temperature range (K)	Observed % weight loss
1	318 to 533	49.26
2	537 to 635	19.10
3	637 to 789	5.03
Total weight loss		73.39

Table 2

Elemental carbon analysis

Temperature of calcination ( $^\circ\text{C}$ )	Percentage of carbon present
500 (15 min)	20
500 (30 min)	4
500 (60 min)	–
600 (15 min)	–

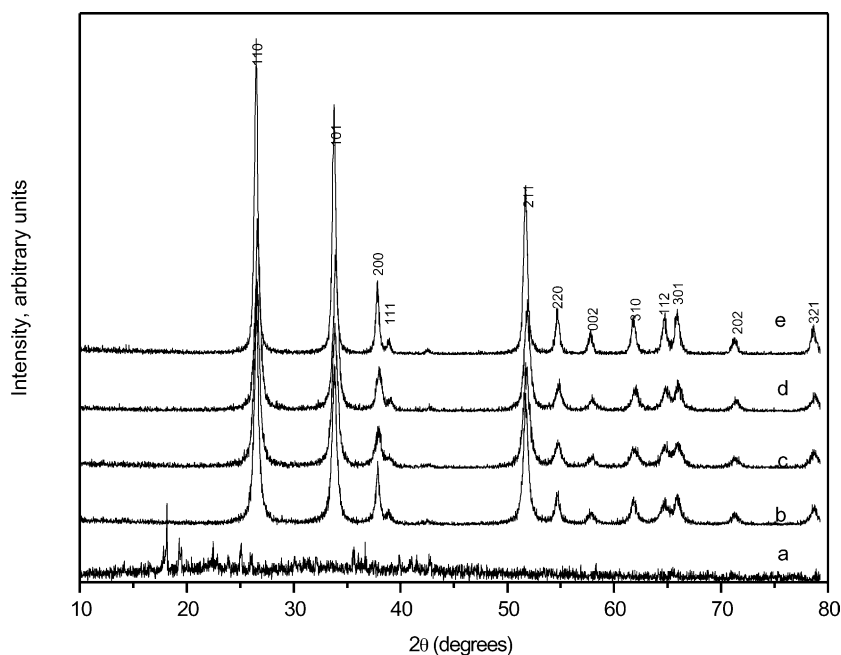


Fig. 3. Powder XRD patterns: a = metal citrate glass; b to e = sample calcined at 873, 973, 1073 and 1173 K, respectively.

the removal of carbon. The product obtained is off-white in color and the intensity of the color changes with the increase in the temperature of calcination.

The thermograms and the differential thermograms of the samples are given in Fig. 2. The observed weight losses at various temperature ranges are given in Table 1. The thermogram of the citric acid (Fig. 2a) used as the citrate precursor shows a major decomposition in the temperature range 318 to 523 K. A small decomposition in the range 823 to 923 K could be due to the decomposition of any carbonaceous matter left behind. However, thermogram of the citrate glass (Fig. 2b) shows decomposition in three steps, which are continuous. The major one is in the

range of 318 to 533 K, followed by another large decomposition steps between 537 and 635 K and a small one between 637 and 789 K. This difference in the decomposition pattern of the citrate glass from the citric acid decomposition clearly indicates the formation of a tin citric acid complex. Similar decomposition patterns have been reported earlier where formation of tin citrate complexes was observed [24]. The total weight loss observed is around 73.39%. Expected weight loss for such a mixture of tin chloride and citric acid is about 58.80%. The excess weight loss observed in the thermogram of the tin citrate glass could be because of the water molecules trapped in the citrate complex glass.

Table 3  
Lattice parameters and specific surface area data obtained from powder XRD

Sample	Crystallinity area under the peaks	Lattice parameters			Crystallite size $D$ (nm)	Specific surface area ( $\text{m}^2/\text{g}$ )
		$a$ ( $\text{\AA}$ )	$c$ ( $\text{\AA}$ )	$V$ ( $\text{\AA}^3$ )		
Sn-600	2769	4.7428	3.1801	71.533	13.48	68.75
Sn-700	2669	4.7405	3.1771	71.397	14.28	64.88
Sn-800	2660	4.7386	3.1779	71.357	15.46	62.91
Sn-900	2785	4.7428	3.1814	71.563	25.23	41.43
ASTM data	—	4.7380	3.1880	71.566	—	—

Carbon analysis data are given in Table 2. The data show about 20% carbon in the sample calcined at 773 K for 15 min, 4% carbon in the sample calcined at 773 K for 30 min and no carbon in the samples calcined at 773 K for 1 h and those calcined at higher temperatures. The data suggest complete decomposition of the citrate glass at temperature as low as 773 K to form SnO<sub>2</sub> free from carbon, whereas carbon residue at temperature as high as 1073 K was reported for metal oxide synthesis using a similar route [19].

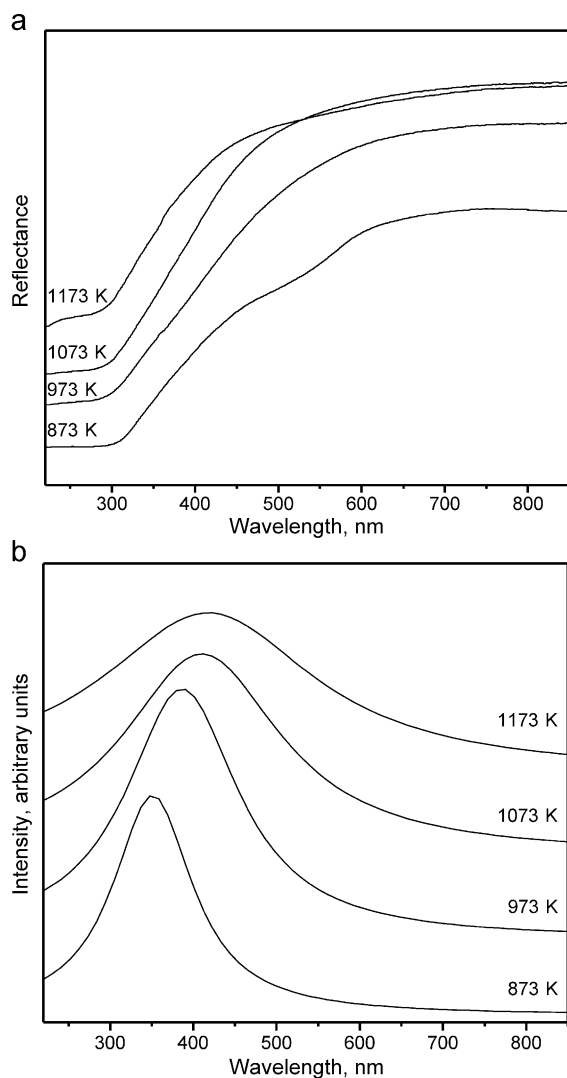


Fig. 4. (a) Diffused reflectance UV–Visible spectra of the samples calcined at different temperatures. (b) Differential plot of the UV–Visible spectra.

Table 4  
Band gap energies of SnO<sub>2</sub> samples calcined at different temperatures

Calcination temperature (K)	Crystallite size (nm)	$\lambda$ (nm)	Band gap energy (eV)
873	13.5	351	3.55
973	14.3	387	3.20
1073	15.5	410	3.11
1173	25.2	418	2.96

The multiple plots of the powder XRD patterns of the various samples are given in Fig. 3. Fig. 3a shows the XRD pattern of the tin citrate complex glass. Some reflections corresponding to anhydrous citric acid can be observed. The large, broad background confirms the highly amorphous nature of the glass. The XRD patterns of the glass samples calcined at 873, 973, 1073 and 1173 K, respectively, are shown in Fig. 3 patterns, b to e. The powder X-ray diffraction patterns confirm the presence of single phase SnO<sub>2</sub> in rutile structure (tetragonal system) for all the samples calcined at different temperatures. Table 3 gives the crystallite size and lattice parameters obtained from the powder XRD data. From the crystallite size data it can be seen that the polycrystalline material has the crystals in the nanometer range from 13 to 25 nm.

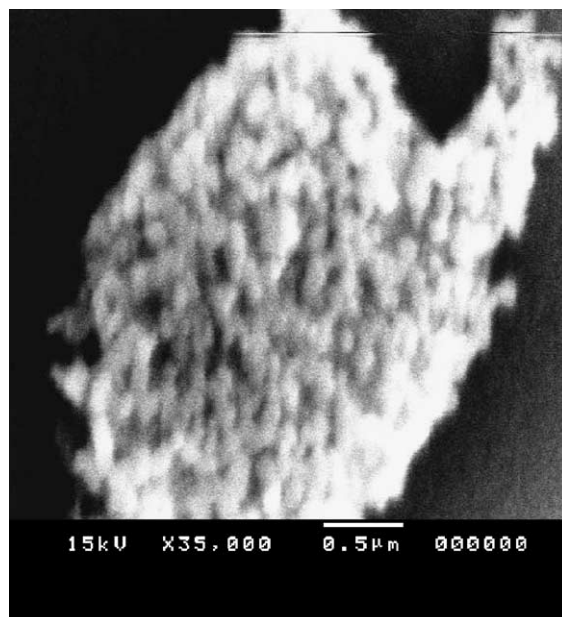


Fig. 5. Scanning electron micrograph of the sample calcined at 873 K.

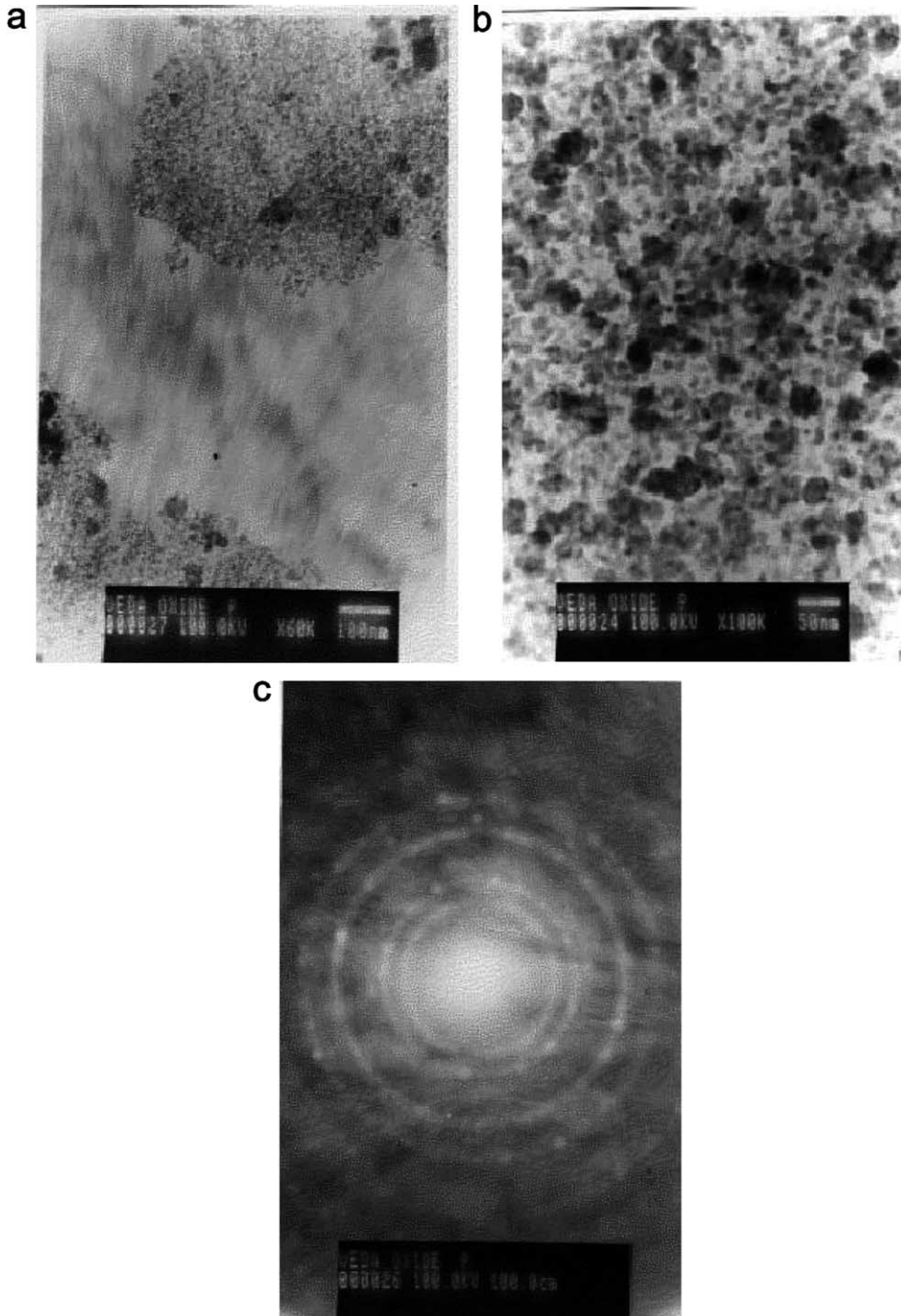


Fig. 6. (a) TEM micrographs of the sample calcined at 873 K. (b) TEM micrographs of the sample calcined at 873 K. (c) Electron diffraction pattern of the sample calcined at 873 K.

There is a gradual increase in the crystallite size of the samples with increase in calcination temperature from 873 to 1073 K, indicating that there are ‘no sintering effects’. Considerable increase in the particle size at 1173 K indicates sintering of the particles at higher temperature. The lattice parameter data shows that the  $a$  value is slightly higher and the  $c$  value is slightly lower for all the samples than reported in the ASTM data. Change in the lattice parameter values as a function of temperature cannot be observed. Even the crystallinity of the sample is observed to be independent of the temperature of calcination. Thus, the material seems to have good thermal resistance properties.

The multiple plots of the diffused reflectance UV–Visible spectra of the samples calcined at 873, 973, 1073 and 1173 K are showed in Fig. 4a. A clear blue shift can be observed in the UV–Visible spectra of the samples as a function of temperature, which can be attributed to the differences in their particle sizes and the slight variations in the color of the samples (from white to off white). The plots of Kubelka–Munk function  $F(R)=(1-R^2)/2R$  (calculated from the diffused reflectance data) vs. wavelength were differentiated to obtain the absorbance maxima values, which were used to calculate the band gap energies. The differential curves are given in Fig. 4b. The band gap energy, determined from the absorbance maxima decreases as crystallite size, determined from the powder XRD data, increases (Table 4).

The SEM micrograph of the sample calcined at 873 K is shown in Fig. 5. It shows an aggregate of very fine particles that cannot be virtually distinguished or measured using a scanning electron microscope. The scale given at the bottom of the Figure indicates that the sample has particles with size less than even 0.1  $\mu\text{m}$ , i.e. 100 nm indicating that the particles are nanoparticles. Fig. 6a–c shows the TEM micrographs of the  $\text{SnO}_2$  sample calcined at 873 K at different magnifications and the electron diffraction pattern, which confirms the nanometric size of the particles. The micrograph shows a homogeneous distribution of the particles, which appear spherical in nature. Most of the particles appear to have a particle size of about 12 to 13 nm and distribution is represented in the histogram given in Fig. 7. The average particle size obtained by a Gaussian fit of the histogram is about 12 nm having a standard deviation of 3 nm, which agree

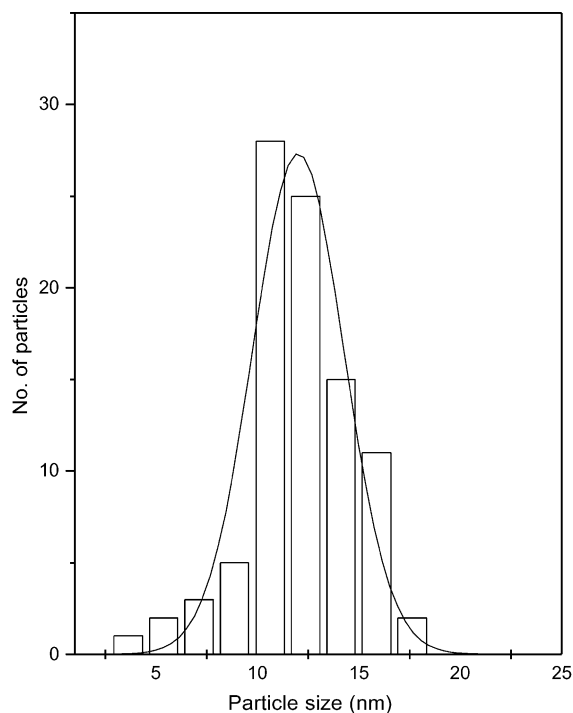


Fig. 7. Average particle size distribution from TEM.

very well with that obtained by powder XRD data. Though some larger particles can be seen, they are likely to be aggregates of the still smaller particles. This indicates that most of the particles falling in this range are as good as single crystals. Assuming the spherical nature of the particles, the specific surface area of the samples has been calculated by using the crystallite size, which is given in Table 3. The sample calcined at 873 K has a surface area of 68.8  $\text{m}^2/\text{g}$ . It decreases as a function of temperature (41.4  $\text{m}^2/\text{g}$  for sample calcined at 1173 K).

#### 4. Conclusions

Nanocrystalline tin oxide can be effectively prepared by the liquid mix technique using citric acid as the complexing agent. The method is simple, cost-effective and less time-consuming. The oxide particles are spherical having a fairly narrow distribution around 12.5 nm supported by both TEM and powder XRD results. The material obtained has good thermal resistant properties.

## Acknowledgements

Authors are grateful to Ms. Renu Parishcha for the Transmission Electron Micrographs, Mrs. Nalini Jacob for the thermal analysis, Dr. S.D. Sathaye for fruitful discussions and Dr. A.V. Ramaswamy for constant encouragement. The authors are thankful to the Department of Science and Technology, New Delhi for financial support.

## References

- [1] T. Maekawa, J. Tamaki, N. Miura, N. Yamazoe, S. Matasushima, *Sens. Actuators*, B 9 (1992) 63–69.
- [2] P. Romppainen, V. Lantto, S. Leppavuori, *Sens. Actuators*, B 1 (1990) 73–78.
- [3] R. Sanjines, V. Demarne, F. Levy, *Thin Solid Films* 193/194 (1990) 935–942.
- [4] D. Kohl, *Sens. Actuators* 18 (1989) 71–114.
- [5] J. Tamaki, T. Maekawa, N. Miura, N. Yamazoe, *Sens. Actuators*, B 9 (1992) 197–203.
- [6] G.S.V. Coles, G. Williams, B. Smith, *J. Phys.*, D, *Appl. Phys.* 24 (1991) 633–641.
- [7] A. Dieguez, J.L. Alay, J. Kappler, A. Romano-Rodriguez, A. Vila, N. Barsan, U. Weimar, W. Gopel, J.R. Morante, *Mater. Res. Soc. Symp. Proc.* 501 (1998) 53–58.
- [8] C. Wang, Y. Hu, Q. Yitai, Z. Guiwen, *Nanostruct. Mater.* 7940 (1996) 421–427.
- [9] L. Fraigi, D.G. Lamas, De Reca, N.E. Walsoe, *Nanostruct. Mater.* 11 (3) (1999) 311–318.
- [10] M.D. Shaji Kumar, T.M. Shrinivasan, P. Ramasamy, C. Subramanian, *Mater. Lett.* 25 (3,4) (1995) 171–174.
- [11] R.E. Juarez, D.G. Lamas, G.E. Lascalea, De Reca, N.E. Walsoe, *J. Eur. Ceram. Soc.* 20 (2) (2000) 133–138.
- [12] L.A. Chick, L.R. Pederson, G.D. Maupin, J.L. Bates, L.E. Thomas, G.J. Exarhos, *Mater. Lett.* 10 (1–2) (1990) 6–12.
- [13] L.R. Pederson, G.D. Maupin, W.J. Weber, D.J. McReady, R.W. Stephens, *Mater. Lett.* 10 (9–10) (1991) 437–443.
- [14] E. Zhou, S. Bhaduri, S.B. Bhaduri, *Ceram. Eng. Sci. Proc.* 18 (4) (1997) 653–660.
- [15] A.K. Shukla, V. Sharma, N. Arul Dhas, K.C. Patil, *Mater. Sci. Eng.*, B B40 (2–3) (1996) 153–157.
- [16] K.R. Venkatachari, D. Huang, P. Steven Ostrander, A. Walter Schulze, C. Gregory Stangle, *J. Mater. Res.* 10 (3) (1995) 748–755.
- [17] L.B. Fraigi, D.G. Lamo, N.E. Walsoe de Reca, *Mater. Lett.* 47 (2001) 262–266.
- [18] M.P. Pechini, U.S. Patent, 3,330,697 (1967).
- [19] M.S.G. Baythoun, F.R. Sale, *J. Mater. Sci.* 17 (1982) 2757–2769.
- [20] C. Marilly, P. Courty, B. Delmon, *J. Am. Ceram. Soc.* 83 (1) (1970) 56.
- [21] N.H. Cahn, R.K. Sharma, *J. Electrochem. Soc.* 128 (1981) 1762.
- [22] N.H. Cahn, D.M. Smyth, *J. Electrochem. Soc.* 123 (1976) 1584.
- [23] D.M. Smyth, *J. Solid State Chem.* 24 (3.4) (1978) 235.
- [24] A. Shrivastava, V.G. Gunjikar, A.P.B. Sinha, *Thermochim. Acta* 117 (1987) 201–217.